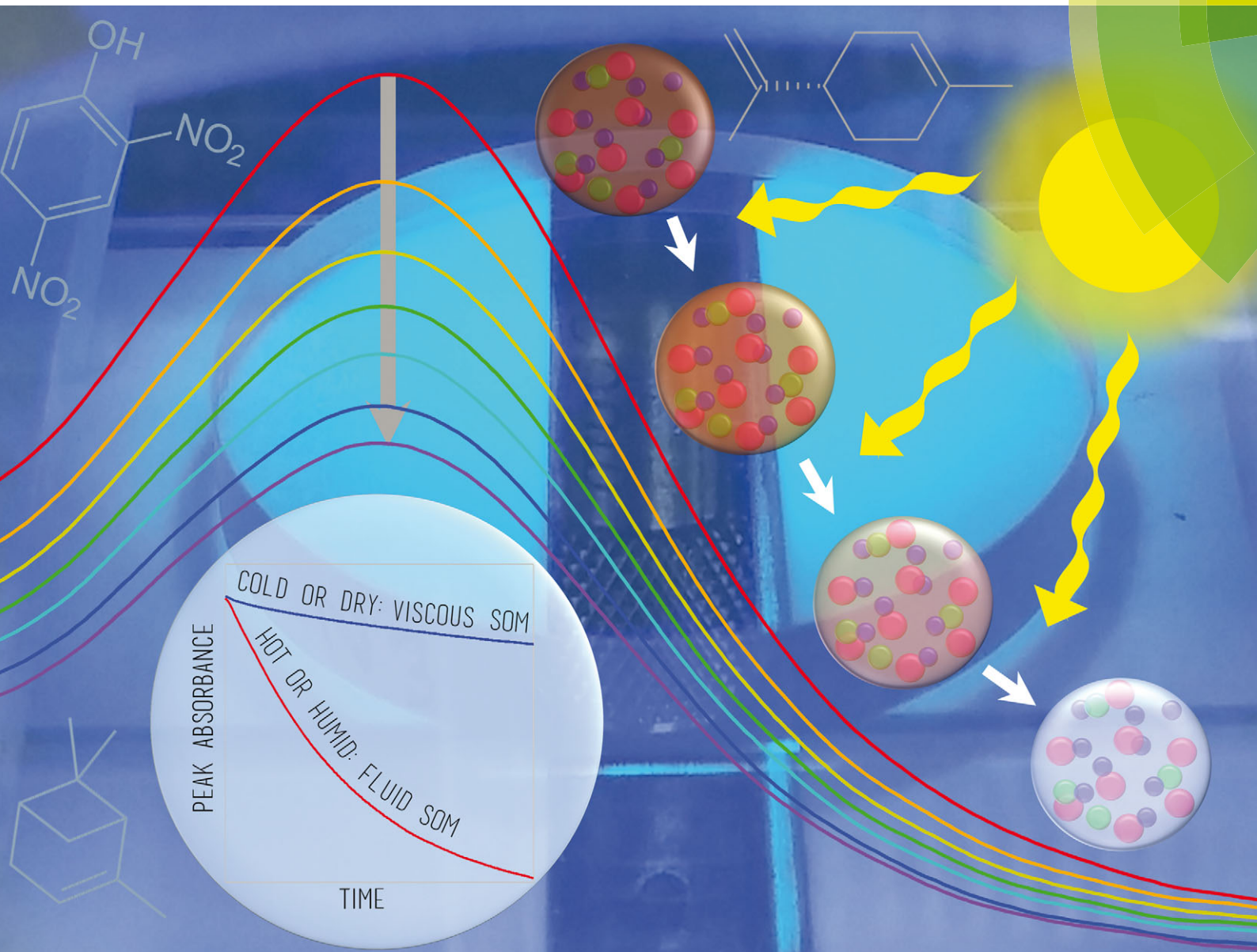


PCCP

Physical Chemistry Chemical Physics

www.rsc.org/pccp



ISSN 1463-9076



ROYAL SOCIETY
OF CHEMISTRY

PAPER

Sergey A. Nizkorodov *et al.*
Effect of viscosity on photodegradation rates in complex secondary organic aerosol materials

175
YEARS



Cite this: *Phys. Chem. Chem. Phys.*,
2016, **18**, 8785

Effect of viscosity on photodegradation rates in complex secondary organic aerosol materials†

Mallory L. Hinks,^a Monica V. Brady,^a Hanna Lignell,^a Mijung Song,^b
James W. Grayson,^b Allan K. Bertram,^b Peng Lin,^c Alexander Laskin,^c
Julia Laskin^d and Sergey A. Nizkorodov^{*a}

This work explores the effect of environmental conditions on the photodegradation rates of atmospherically relevant, photolabile, organic molecules embedded in a film of secondary organic material (SOM). Three types of SOM were studied: α -pinene/O₃ SOM (PSOM), limonene/O₃ SOM (LSOM), and aged limonene/O₃ obtained by exposure of LSOM to ammonia (brown LSOM). PSOM and LSOM were impregnated with 2,4-dinitrophenol (2,4-DNP), an atmospherically relevant molecule that photodegrades faster than either PSOM or LSOM alone, to serve as a probe of SOM matrix effects on photochemistry. Brown LSOM contains an unidentified chromophore that absorbs strongly at 510 nm and photobleaches upon irradiation. This chromophore served as a probe molecule for the brown LSOM experiments. In all experiments, either the temperature or relative humidity (RH) surrounding the SOM films was varied. The extent of photochemical reaction in the samples was monitored using UV-vis absorption spectroscopy. For all three model systems examined, the observed photodegradation rates were slower at lower temperatures and lower RH, conditions that make SOM more viscous. Additionally, the activation energies for photodegradation of each system were positively correlated with the viscosity of the SOM matrix as measured in poke-flow experiments. These activation energies were calculated to be 50, 24, and 17 kJ mol⁻¹ for 2,4-DNP in PSOM, 2,4-DNP in LSOM, and the chromophore in brown LSOM, respectively, and PSOM was found to be the most viscous of the three. These results suggest that the increased viscosity is hindering the motion of the molecules in SOM and is slowing down their respective photochemical reactions.

Received 1st September 2015,
Accepted 7th December 2015

DOI: 10.1039/c5cp05226b

www.rsc.org/pccp

Introduction

Recent investigations into the phase state of secondary organic aerosol (SOA) have suggested that under certain conditions, both atmospheric and laboratory-generated SOA particles may behave as semi-solids or amorphous solids rather than liquids.^{1–6} This realization has important implications for our understanding of processes occurring within SOA material. The rheological properties of organic aerosols, such as viscosity, are expected to play a role in the dynamics of particle growth,^{6,7} gas-particle partitioning,^{8–10} diffusion kinetics of water, oxidants, and other compounds,^{11–15} the dynamics of particle aggregation,¹⁶ and reactive uptake on particle surfaces.^{17–20} Diffusion limitations

imposed by the increased viscosity of SOA have already been shown to impact the particle growth rates and mechanisms as well as the oxidation rates of organics within the SOA.^{2,6,9,12,13}

Environmental conditions such as temperature and relative humidity (RH) are expected to have a significant effect on the viscosity of SOA particles.^{1–3,11,13,16,21–24} As either temperature or RH of the system is increased, the secondary organic material (SOM) from which the particle is made will decrease in viscosity. For example, Renbaum-Wolff *et al.* reported that the viscosity of α -pinene/O₃ SOM increases by several orders of magnitude upon reducing the RH from 90% to 30%.³ The effect of temperature on the viscosity of SOM has not yet been studied, but we estimate that a decrease in temperature from 20 °C to 0 °C will decrease the viscosity of α -pinene/O₃ SOM by roughly two orders of magnitude, as discussed in our previous work.²⁵

The goal of this work is to investigate the effect of SOM matrix properties on the photochemical kinetics of photolabile, organic molecules within the SOM by varying the temperature and RH. Experiments were performed on three types of organic matrix including α -pinene/O₃ SOM (PSOM), limonene/O₃ SOM (LSOM), and aged limonene/O₃ SOM obtained by exposure of

^a Department of Chemistry, University of California, Irvine, CA 92697, USA.
E-mail: nizkorod@uci.edu

^b Department of Chemistry, University of British Columbia, Vancouver, BC, Canada

^c Environmental Molecular Sciences Laboratory, Pacific Northwest National Laboratory, Richland, WA 99352, USA

^d Physical Sciences Division, Pacific Northwest National Laboratory, Richland, WA 99352, USA

† Electronic supplementary information (ESI) available. See DOI: 10.1039/c5cp05226b

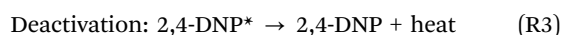
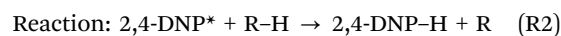
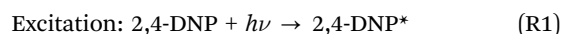
LSOM to ammonia (brown LSOM). These particular systems were selected for two main reasons. First, PSOM and LSOM are common SOA materials in both outdoor and indoor environments: α -pinene is the most important precursor to global SOA and limonene is the most important indoor SOA precursor.^{26,27} Second, brown LSOM was selected to test both the effect of exposure to ammonia on the viscosity of LSOM and to examine a different type of photochemistry. (We did not do experiments with PSOM exposed to ammonia because reaction of PSOM with ammonia, unlike that of LSOM, does not lead to browning.)²⁸ Although the elemental composition of LSOM and PSOM components is quite similar, with average O/C ratios of 0.39 and 0.37 respectively, the viscosity of PSOM is likely to be greater than that of LSOM because the products of α -pinene ozonolysis tend to be more structurally rigid.^{29,30} Similarly, brown LSOM may be physically and chemically different from LSOM because it contains products of reactions of NH_3 with carbonyls.³⁰ Understanding how viscosity of SOA may play a role in the photochemical kinetics of different types of atmospheric molecules trapped within them is important in order to better predict the lifetimes of toxic pollutants.

Ideally, these experiments should be done with submicron aerosol particles, similar to the ones found in the atmosphere, in order to maintain the correct time scale for the gas-to-particle exchange of volatile products and reactants (*e.g.*, molecular oxygen dissolved in the particles) of the photochemical processes occurring in particles. However, experiments performed with aerosol particles would be more difficult and suffer from potential interference from competing gas-phase photochemical processes.³¹ We have chosen to simplify the experiments by working with the bulk phase of SOM collected on a substrate. For photochemical reactions that involve only condensed-phase reactants and products, bulk SOM experiments should provide the same information as experiments with aerosols.

As PSOM and LSOM photodegrade relatively slowly, a strongly absorbing, nitroaromatic pollutant 2,4-dinitrophenol (2,4-DNP) was dispersed in the SOM films to serve as a photochemical probe molecule. This compound enters the environment predominantly from pesticide use, manufacturing plants, biomass burning, and motor vehicles.^{32–35} It is known to be present in surface and atmospheric waters and in organic matter. Although mixing of 2,4-DNP and biogenic SOA is unlikely, we used 2,4-DNP just as a probe of SOM matrix effects on photochemistry. The photodegradation of 2,4-DNP upon UV irradiation is accompanied by a decay in its absorbance at 290 nm and an increase in absorbance in the visible region of the spectrum, where PSOM and LSOM do not absorb, due to the formation of photo-products.²⁵

2,4-DNP is expected to photodegrade by a mechanism shown in reactions (1)–(4). As 2,4-DNP is irradiated, it is excited to a triplet state (reaction (1)) and proceeds to abstract a hydrogen atom from a neighboring molecule possessing weakly-bound hydrogen atoms (reaction (2)). Saturated hydrocarbons, aromatic hydrocarbons, and water are not suitable hydrogen donors in this reaction, whereas alcohols and aldehydes readily participate in the H-atom transfer. We assume that the rate of reaction (2) may

be diffusion (and thus viscosity) limited. Diffusion limitations in a more viscous matrix would allow more time for competing deactivation (reaction (3)) to occur, thus preventing formation of 2,4-DNP photoproducts (reaction (4)). For example, 2,4-DNP* would need just a few nanoseconds to diffuse 0.6 nm (a reasonable estimate for the distance to the closest abstractable H-atom) in a moderately viscous solvent such as octanol (viscosity $\sim 7 \times 10^{-3}$ Pa s), but it would need several milliseconds to diffuse the same distance in PSOM (viscosity $\sim 10^4$ Pa s). The latter time is more than sufficient for the dissipation of the electronic excitation energy into heat. The excited states lifetime of 2,4-DNP has not been reported, but based on the triplet lifetimes of related nitrobenzene and nitrophenols (*ortho*, *meta*, and *para*) determined by Takezaki *et al.* we expect it to be < 1 ns.³⁶ Therefore, diffusion limitations may arise in materials with viscosity comparable to that of PSOM.



Our previous study examined the photochemistry of 2,4-DNP at a range of temperatures in three different environments: water, octanol, and PSOM.²⁵ It was found that the rate of photochemical degradation of 2,4-DNP in PSOM was more strongly affected by temperature than the same reaction in octanol. We proposed that viscosity of the matrix is a key factor affecting the rates of photoreactions occurring in PSOM. However, other interpretations of the observations could not be excluded, for example, a different reaction mechanism in PSOM compared to octanol. To further investigate the possible matrix effects on the photochemistry of 2,4-DNP, we extended our measurements to various temperatures and RHs in two different types of matrices – PSOM and related material LSOM.

The third system examined in this study is brown LSOM formed by exposing fresh LSOM to ammonia vapors and drying the sample. It has a distinctive absorption band at 510 nm that, in combination with tails of UV absorption bands extending into the blue region of the spectrum, give the material a characteristic brown color.^{30,37–40} Lee *et al.* found that an aqueous solution of brown LSOM readily photobleaches after several minutes of exposure to UV radiation; the peak at 510 nm decays and the brown color disappears.²⁸ Because this system photodegrades quickly and possesses a distinct UV-absorbing functionality, an additional probe molecule was not used. Although the molecular nature of the actual chromophore is not presently known, it is likely to be an oligomeric, nitrogen containing compound formed by condensation reactions between SOA carbonyls and ammonia.³⁰

We find that all three model systems exhibit similar behavior wherein the photodegradation rate is increased at higher temperature or higher RH. While the temperature effects can result from a number of factors, the fact that there is also an RH dependence suggests that viscosity is an important factor in

photochemical reactions taking place within matrices. Increased viscosity may be hindering the motions of the molecules in the SOM and therefore slowing down the photochemical reactions in which they participate.

Experimental

SOM for each experiment was generated in a 20 L flow tube by dark ozonolysis of an SOA precursor volatilized under a flow of dry air. Typical mixing ratios in the flow tube were 70 ppm for O_3 and 10 ppm for the precursor, either α -pinene (98%, Alfa Aesar) or limonene (97%, Sigma-Aldrich); the flow tube residence time was about 4 minutes. After passing through a charcoal denuder to eliminate excess ozone and organic vapors, the particles were collected using a Sioutas slit impactor (Cat. No. 225-370) equipped with a single stage D (0.25 μm cut point at 9 SLM collection flow rate), which was customized to accommodate 25 mm CaF_2 windows as the impaction substrates. The average collection time of 45 minutes generally produced about 2 mg of SOM deposited on the window.

For the first two sets of experiments (PSOM/2,4-DNP and LSOM/2,4-DNP), 2,4-DNP (99.4%, Sigma Aldrich) was added to SOM by pipetting 100 μL of a 0.01 M 2,4-DNP/methanol solution onto the CaF_2 window, partially dissolving the SOM. The methanol was allowed to evaporate and 2,4-DNP to permeate the SOM for 30 minutes, after which the 2,4-DNP remained embedded in a thin film of SOM (as far as we could ascertain based on the inspection of the film under optical and Raman microscopes). It was necessary to keep the concentration of embedded 2,4-DNP low enough to ensure that the viscosity of the SOM matrix was not significantly affected, yet also high enough to absorb more radiation than the surrounding SOM molecules. Therefore, we elected to use a mass ratio of 2,4-DNP:SOM around 1:50 to satisfy both requirements.²⁵

For the third set of experiments, brown LSOM was produced by exposing fresh LSOM to ammonia vapors as described in ref. 37. First, a thin film of LSOM was created by pipetting 100 μL of methanol onto the LSOM, allowing it to spread over the window, and evaporating the solvent for 30 minutes. The window was then inserted into a small glass petri dish, which was placed carefully into a larger petri dish containing a solution of 0.1 M ammonium sulfate (>99%, EMD) thus allowing it to absorb the vapors (estimated to contain 300 ppb NH_3 using the AIM-II model),⁴¹ but not touch the actual solution. The larger petri dish was covered with a lid and the entire unit was stored in the dark. After two days of exposure, the window was removed and dried under a flow of dry air for at least one hour, after which the SOM film had browned.

After each sample (2,4-DNP in SOM or brown LSOM) was prepared, it was irradiated inside the temperature and RH controlled setup shown in Fig. 1. The CaF_2 window loaded with sample was placed on top of a quartz microscope slide that was maintained at a desired temperature ranging from 0 $^\circ\text{C}$ to 35 $^\circ\text{C}$ using a circulating water cooler connected to an aluminum heat sink. If needed, in order to achieve temperatures below

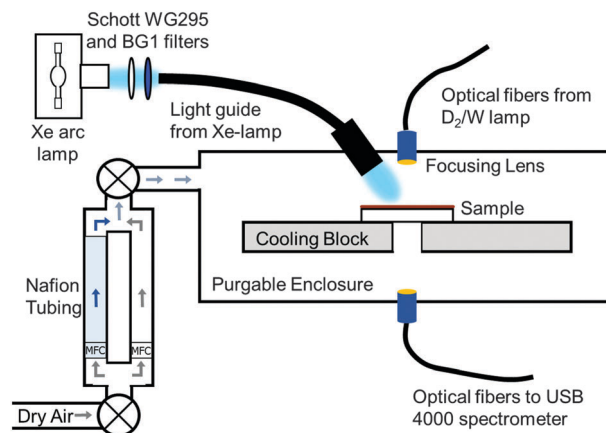


Fig. 1 A schematic diagram of the relative humidity- and temperature-controlled photoreaction box used to irradiate all samples at various RH and temperatures.

5 $^\circ\text{C}$, two Peltier coolers (TE Technology, Inc. TC-48-20) were utilized in addition to the water cooler. The temperature was monitored throughout the experiment using a type-K thermocouple mounted on the microscope slide.

The RH within the box was controlled by mixing flows of dry (<2% RH) and wet (>98% RH) air. Incoming dry air was first split into two separate flows controlled by two mass flow controllers. The humidified flow was obtained by passing dry air through a Nafion drier/humidifier (PermaPure). The final RH was set by adjusting the flow through each mass flow controller. The RH inside the box was measured with a Vaisala HMP237 probe.

Irradiation of each sample was performed with the output of a 150 W xenon arc lamp (Newport model 66902 lamp housing) that was reflected by a 280–400 nm dichroic mirror and passed through a 295 nm long-pass filter (Schott WG295) and UV band-pass filter (Schott BG1) in order to isolate a band (290–400 nm) of the actinic radiation that is most relevant for tropospheric photochemistry. The light was then piped into the photoreaction box through a liquid light guide (Edmunds #53-691) at a 15 $^\circ$ angle with respect to the film normal (see Fig. 1).

Absorption spectra of the SOM film were recorded using a custom spectrometer setup consisting of a D_2/W light source and an Ocean Optics USB4000 spectrometer. The radiation from the light source was transmitted between spectrometer components and across the sample using 600 μm optical fibers as is shown in Fig. 1.

Viscosity measurements of SOM were performed using the poke-flow technique described in ref. 3, 23 and 42. The method builds on the qualitative approach introduced by Murray *et al.* to determine the flow characteristics of particles.⁴³ Briefly, SOM was generated in the 20 L flow tube as described above and collected using the Sioutas impactor on substrates coated with trichloro(1*H*,1*H*,2*H*,2*H*-perfluorooctyl)silane (Sigma-Aldrich). The coating procedure is described in detail in ref. 44. During collection, the aerosol particles from the flow tube coagulated on the hydrophobic substrates creating supermicron SOM particles. After collection, the substrates containing the supermicron

particles were transported to the University of British Columbia and stored at ~ 280 K until the viscosity measurements were carried out.

The supermicron SOM particles on the hydrophobic substrates were placed inside a RH-controlled flow-cell to carry out viscosity measurements.^{44–46} The flow-cell contained a small hole in the top, which allowed a sterilized sharp needle (0.9 mm \times 40 mm with a 10 μ m tip, Becton-Dickson, USA) to pass through and poke the particles. The needle was mounted on a micromanipulator (Narishige, model MO-202U, Japan) allowing precise control of the movement of the needle. Prior to poking, the geometry of a particle was a spherical cap. Due to the force by the needle while poking, the spherical cap geometry was converted into a half-torus geometry. After the needle was removed, the material flowed to minimize the surface energy of the system and eventually returned back to the spherical cap geometry by filling the central hole. This process was monitored and recorded using a reflectance optical microscope (Zeiss Axio Observer, 40 \times objective) equipped with a CCD camera. The diameter of the equivalent hole area produced by poking the particle was calculated based on the relationship $d = (4A/\pi)^{1/2}$, where d is the equivalent area diameter of a hole with area A .⁴⁷ The experimental flow time, $\tau_{(\text{exp,flow})}$, was determined as the time needed for d to reach half of the initial value of the inner hole of the half torus.

Simulations of fluid flow were carried out using COMSOL Multiphysics (version 4.3a) to convert $\tau_{(\text{exp,flow})}$ values into viscosity.^{23,42} In the simulations, a half-torus geometry with an inner radius, R , and a tube radius, r , were required. These values were set to match the experiments, and the viscosity was varied until the modeled flow time, $\tau_{(\text{mod,flow})}$, was equal to $\tau_{(\text{exp,flow})}$. The physical parameters needed for these simulations include: slip length (the interaction between the fluid and solid surface), surface tension and density of the SOM, and the contact angle at the particle–substrate interface. Upper and lower limits of the parameters used in these simulations are provided in Table 1. Previous validation experiments with sucrose–water particles and high viscosity standards have shown that the poke-flow technique combined with simulations

of fluid flow is capable of providing both lower and upper limits of viscosity that are consistent with literature or measured values when the viscosity of particles are in the range of 5×10^2 to 3×10^6 Pa s.⁴² The major source of uncertainty in the viscosity of the SOM arises from uncertainty in the physical properties of SOM that are used in simulations (*i.e.*, values shown in Table 1). Particle to particle variability of $\tau_{(\text{exp,flow})}$ is typically small.

Results and discussion

The absorption spectra of (a) 2,4-DNP in LSOM and (b) brown LSOM taken during the course of photodegradation are presented in Fig. 2. The inset of each graph corresponds to the absorbance decay at the representative wavelength for each system (290 nm for 2,4-DNP in LSOM and 510 nm for brown LSOM). The combined absorbance from the SOM and the reactant can be expected to follow eqn (1),

$$A(t) = A_{\text{SOM}} + A_0[\beta + (1 - \beta) \times e^{-kt}] \quad (1)$$

where A_{SOM} is the absorbance due to the SOM matrix, assumed to be unchanged by photolysis, A_0 is the starting absorbance due to the reactant, k is the photodegradation rate constant, and β is the ratio of the absorption coefficient of the photolysis product(s) to that of the reactant at the wavelength of interest. (The value of β is 0 for non-absorbing products, smaller than 1 for weakly absorbing products, 1 at the isosbestic point, and larger than 1 when products absorb stronger than the starting compound.) Since we were interested only in the values of k , the observed decays were fit using the simplified equation:

$$A(t) = \text{const}_1 + \text{const}_2 + e^{-kt} \quad (2)$$

to obtain rate constants for each set of experimental conditions. The use of eqn (2) automatically accounts for any uncompensated wavelength-independent offsets in the absorbance measurements.

It should be noted that in the case of 2,4-DNP, the decay in absorbance at ~ 250 – 320 nm is accompanied by an increase in the broad absorption band in the visible range (~ 400 – 450 nm) indicating formation of a brown carbon product (a result of

Table 1 Physical parameters used in the simulations to determine viscosities of α -pinene-derived SOM (PSOM) and limonene-derived SOM (LSOM). R and r indicate the radius of the tube and the radius of the inner hole, respectively, for a half-torus geometry

		Slip length ^a (nm)	Surface tension ^b (mN m ⁻¹)	Density ^c (g cm ⁻³)	Contact angle ^d ($^\circ$)
PSOM	Values for lower limit	5	40	1.30	70 (if $r < 2R$), 90 (if $r > 2R$)
	Values for upper limit	10 000	75	1.30	90 (if $r < 2R$), 70 (if $r > 2R$)
LSOM	Values for lower limit	5	23	1.47	60 (if $r < 2R$), 80 (if $r > 2R$)
	Values for upper limit	10 000	72	1.67	80 (if $r < 2R$), 60 (if $r > 2R$)
Brown LSOM	Values for lower limit	5	23	1.47	65 (if $r < 2R$), 80 (if $r > 2R$)
	Values for upper limit	10 000	72	1.67	80 (if $r < 2R$), 65 (if $r > 2R$)

^a Ref. 48–61. ^b For PSOM, surface tension values were based on the viscosity of model compounds.⁶² For LSOM and brown LSOM, surface tension values were based on the estimated surface tension of liquid limonene at 293 K (as the lower limit) and the surface tension of pure water at 293 K (as the upper limit) values from ACD/Labs (chemspider.com) and Engelhart *et al.*⁶³ ^c For PSOM, density values are based on Chen and Hopke, 2009.⁶⁴ For LSOM and brown LSOM, density values are based on values from Kostenidou *et al.*⁶⁵ ^d Contact angles (70–90 $^\circ$ for PSOM and 60–80 $^\circ$ for LSOM) were determined using 3-D fluorescence confocal images of the SOM particles on the substrates.

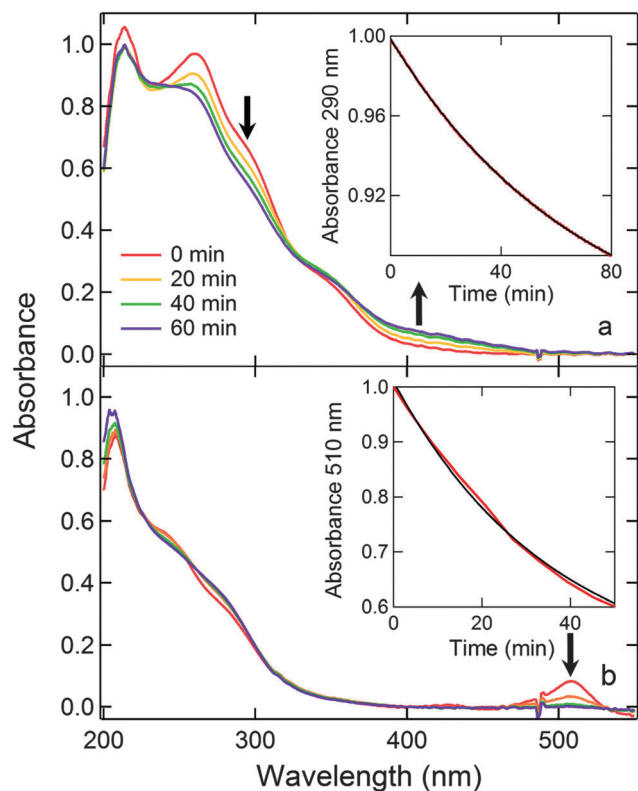


Fig. 2 Representative absorption spectra recorded during the photodegradation of (a) 2,4-DNP in LSOM and (b) brown LSOM. The insets show the decay of (a) the 290 nm peak of 2,4-DNP and (b) the 510 nm peak characteristic of the brown LSOM chromophore where the red trace is the experimental decay and the black trace is the fit to eqn (2). The arrows indicate the wavelength at which the spectra are changing significantly.

reduction of one of the $-\text{NO}_2$ groups to $-\text{NH}_2$ group as discussed below). The rate constants k determined from eqn (1) and (2) at 290 nm (decrease in absorbance, $\beta < 1$, $\text{const}_2 > 0$) and 420 nm (increase in absorbance, $\beta > 1$, $\text{const}_2 < 0$) were the same within the uncertainties of the fitting.

The increase in the visible absorbance of the irradiated 2,4-DNP samples is an important observation for two reasons. First, it confirms recent findings that photochemical processing is capable of altering the light absorption properties of brown carbon.^{28,66,67} Second, it shows that, depending on the system, photochemical processes in brown carbon are capable of creating light-absorbing compounds, not just destroying (photobleaching) them. Our work provides evidence that brown carbon has a dynamic absorption spectrum that can be altered on atmospherically relevant time scales *via* photochemistry.

To investigate the mechanism of 2,4-DNP photodegradation, we performed LC-PDA-MS (liquid chromatography coupled to a photodiode array detector and an electrospray ionization high-resolution mass spectrometer) measurements on irradiated samples of 2,4-DNP in isopropanol (0, 30, and 60 min of irradiation in a quartz cuvette by the same light source as used for the film experiments). Isopropanol was used as the solvent in this analysis, as SOM is very complex and is made up

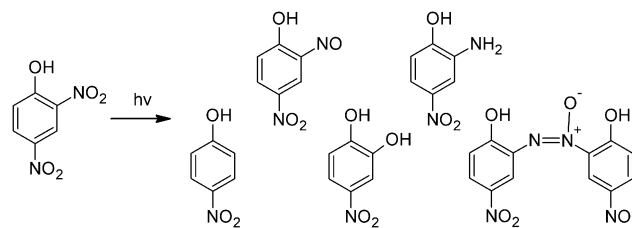


Fig. 3 Products tentatively identified by LC-PDA-MS after 2,4-DNP photolysis in isopropanol. Details leading to the assignments are provided in the ESI.†

of many different molecules that would yield a complicated background spectrum.²⁹ The full results of the LC-PDA-MS analysis, as well as experimental details, are provided in the ESI.† We assigned the observed products of photodegradation of 2,4-DNP by analogy with photochemistry of related compounds, nitrobenzene and 2-nitrophenol. Based on the m/z values and UV-vis absorption spectra of the eluted peaks, we were able to assign products to the structures shown in Fig. 3. We emphasize that we did not have standards for any of these compounds for unambiguous identification, so the assignments should be regarded as tentative. Nevertheless, our results strongly suggest that photoreduction of $-\text{NO}_2$ group(s) in 2,4-DNP is the main mechanism of photodegradation. We observed peaks corresponding to an $-\text{NH}_2$ (aniline) product as well as to an $-\text{NO}$ (nitroso) intermediate which is expected for this process. Based on the UV-vis absorption spectra (Fig. S9 of the ESI†) the compounds containing an aniline group are likely the ones responsible for the brown color of the 2,4-DNP photodegradation products after the irradiation and cause the growth of the visible absorption band at $\sim 400\text{--}450$ nm. The formation of aniline products has significant implications for understanding the environmental fate of 2,4-DNP because of the high reactivity of aniline compounds.

Regarding the kinetics of 2,4-DNP photodegradation, as discussed in Lignell *et al.*,²⁵ the effective activation energy of reactions with low intrinsic barriers is determined by the surrounding matrix's viscosity, which depends strongly on temperature. The photodegradation of 2,4-DNP fits this profile – it has low activation energy in octanol and much higher activation energy in PSOM, likely due to the high viscosity of the PSOM film.²⁵ The activation energy of each system studied in the current work was determined using the Arrhenius plot shown in Fig. 4. This plot illustrates the relationship between temperature and rate constant for each system (including 2,4-DNP in PSOM shown previously in ref. 25) under dry conditions. The results indicate that the activation energy of the photodegradation of 2,4-DNP in LSOM (24 ± 1 kJ mol^{-1}) is lower than that in PSOM (48 ± 6 kJ mol^{-1}). If these activation energies are actually viscosity-dependant, then this suggests that PSOM has a higher viscosity than LSOM. Another observation of the current work is that both of the reactions that occurred in LSOM (2,4-DNP and brown LSOM) had similar activation energies (24 ± 1 kJ mol^{-1} and 16 ± 5 kJ mol^{-1} , respectively) implying that the viscosities of LSOM and brown

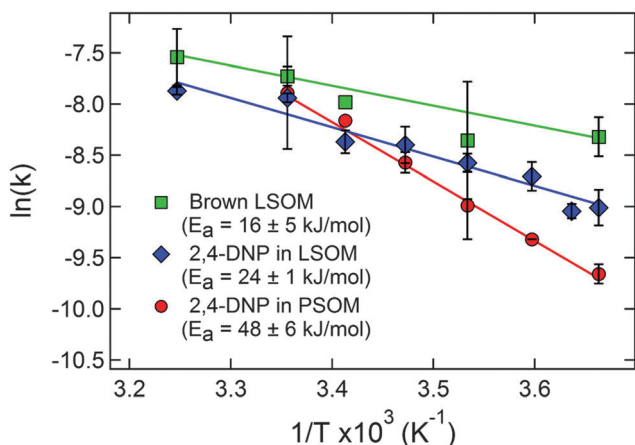


Fig. 4 Arrhenius plots of the photodegradation rate of 2,4-DNP in PSOM (red), 2,4-DNP in LSOM (blue), and brown LSOM (green) under dry conditions. The slopes correspond to activation energies of 48, 24, and 16 kJ mol⁻¹, respectively. Markers with no error bars represent experiments that were performed once. All other markers are the average of 2–6 data points obtained at each temperature.

LSOM are similar. This would be consistent with minor compositional differences between the two materials.⁶⁸

In order to test this hypothesis, the viscosities of LSOM and PSOM generated in our flow tube were experimentally determined from poke flow experiments at different RHs, specifically, by measuring how quickly a half-sphere of SOM returns to its original shape after being distorted by a needle. The results of these experiments are shown in Fig. 5. Fig. 5a depicts the average experimental flow time, which is taken for the equivalent area diameter to decrease to 50% of its initial diameter. The PSOM had a longer experimental flow time than either LSOM or brown LSOM. For example, under dry conditions the experimental flow time of PSOM is longer by approximately an order of magnitude than the experimental flow times of LSOM and brown LSOM, strongly suggesting a higher viscosity. Unlike the clearly different poke flow times in PSOM and LSOM, the error bars on the absolute viscosity values shown in Fig. 5b overlap because of the sensitivity to the model parameters needed to convert the poke flow times into the viscosity values. However, the simulated upper and lower limits of viscosity also suggest that PSOM is more viscous than LSOM or brown LSOM. These results are qualitatively consistent with larger apparent activation energies for the photodegradation of 2,4-DNP in PSOM vs. LSOM.

It is also clear from Fig. 5 that the viscosity of SOM is strongly related to RH, which is in agreement with previous measurements.³ Irradiation of all systems under a range of RHs revealed that as RH was increased, the photoreaction rate constant increased (Fig. 6). The number of data points in Fig. 6 is limited because each point requires several days of experiments, however, the increase in the rate with RH is clear. We interpret this to be the result of water molecules softening the SOM matrix and allowing for the photoexcited molecules to diffuse to their reaction partners faster. We note that liquid–liquid phase-separation (LLPS) is possible in PSOM at very high

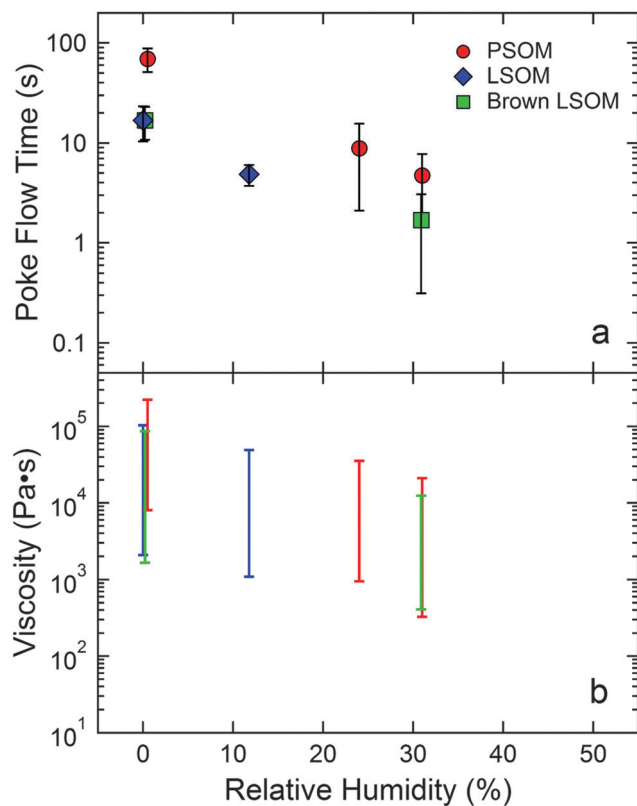


Fig. 5 (a) Average experimental flow time from the poke-flow experiments as a function of relative humidity. The markers correspond to the average of 4–11 individual poke flow measurements. The error bars represent one standard deviation for the repeated measurements. (b) Simulated ranges of viscosities as determined by upper and lower limits. The error bars are dominated by the uncertainties in the fitting parameters listed in Table 1.

RH > 95%,^{69,70} but the increase in the photodegradation rate is also observed at lower RH. Therefore we do not think that LLPS is responsible for the RH dependence of the photodegradation rate. The change of RH seemed to have a larger effect on the brown LSOM system than either of the 2,4-DNP/SOM systems. This is most likely due to the fact that 2,4-DNP photodegrades extremely slowly in water.²⁵ As water molecules are introduced to the film, the rate of photodegradation may be increased due to decreased viscosity, but it is partly offset by the dilution of the molecules that 2,4-DNP can react with. The photodegradation of brown LSOM, on the other hand, is not affected by the presence of water molecules. Therefore, the increase in the rate of photodegradation due to decreased viscosity will be greater for brown LSOM than for 2,4-DNP in LSOM or PSOM which may explain the larger RH dependence seen in brown LSOM.

We should point out that viscosity is not the only property of SOM that can change with RH. It is conceivable that the presence of water in the SOM film changes the molecular composition by means of hydration of aldehydes, hydrolysis of anhydrides, and other reactions involving water. For example, hydrolysis reactions of organonitrates in aerosols have been observed at the RH levels used in this work.⁷¹ While these

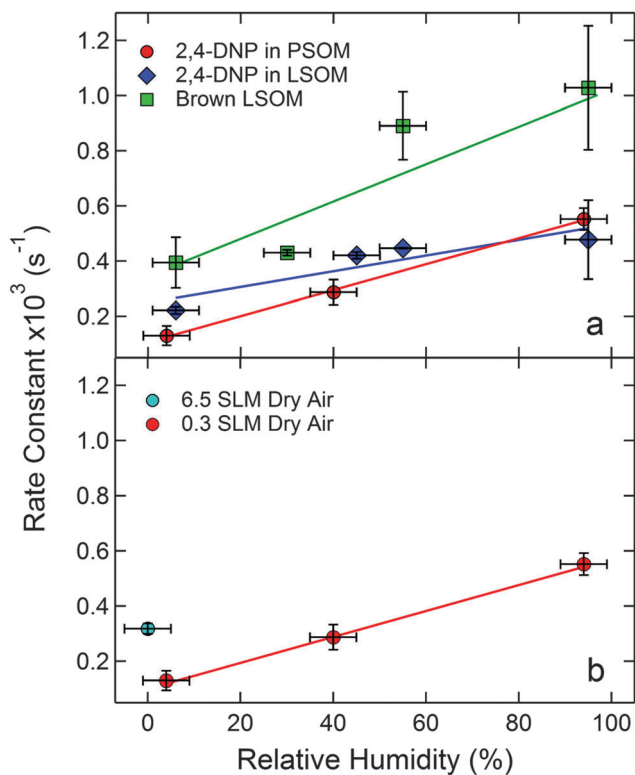


Fig. 6 (a) The rate constants as a function of relative humidity for the photodegradation of 2,4-DNP in PSOM, 2,4-DNP in LSOM, and brown LSOM. Each marker with error bars represents the average of all the data points at each RH. These experiments were repeated 2–6 times. The slopes of the fit were $(4.7 \pm 0.1) \times 10^{-6}$, $(2.9 \pm 0.9) \times 10^{-6}$, and $(8 \pm 2) \times 10^{-6} \text{ s}^{-1}/\% \text{ RH}$ for 2,4-DNP in PSOM, 2,4-DNP in LSOM, and brown LSOM respectively. Plot (b) demonstrates the effect of drying speed.

reactions may also contribute to the observed changes in the photodegradation rate, the physical effect of RH on the SOM viscosity likely dominates over the chemical effect of RH on the molecular composition of SOM. Additional experiments with materials that are not reactive towards water are needed to fully separate the chemical and physical effects of RH.

Koop *et al.* and other groups have previously found that the viscosity of an aerosol particle at a particular RH strongly depends on the rate at which the system is dried/humidified.^{2,72–74} It has been suggested that drying quickly will cause water molecules nearest the surface of the particle to evaporate quickly, creating a highly viscous “crust” that prevents water molecules in the interior of the particle from escaping. This results in an aerosol particle that contains a lower viscosity core.^{2,72} Drying more slowly allows more time for water molecules within the particle to diffuse to the outer layers and evaporate, causing the particle to be more uniform in terms of viscosity. Thus the interior viscosity of the slowly dried particle is actually expected to be higher than that of the interior of the quickly dried particle.

In our studies, the lowest RH experiments were performed under two different flow rates of dry air (6.5 SLM and 0.3 SLM). We found that the samples that were dried under a high flow rate of dry air photodegraded more quickly than samples dried under the slower flow rate. This was a reproducible effect,

demonstrated by Fig. 6b (note the small vertical error bars calculated from the repeated experiments). The red dots correspond to samples of 2,4-DNP in PSOM that were dried/humidified under a 0.3 SLM flow rate, and the light blue dot represents the samples that were dried under a 6.5 SLM flow rate. The fast dried samples with a low viscosity core had a photodegradation rate that was a factor of ~ 3 higher than the slow dried samples with a high viscosity core. This provides additional indirect evidence that the viscosity of SOM plays an important role in the photodegradation of these systems.

These results suggest that certain types of photochemical reactions may be suppressed in condensed-phase environment of the highly-viscous aerosols relative to the same reactions in common organic solvents. In particular, photochemical processes involving secondary reactions of electronically-excited organic molecules with the matrix constituents are likely to be affected by the diffusion limitations, and therefore, by the viscosity. This scenario clearly applies to 2,4-DNP, which photodegrades by a reaction of its triplet excited state with suitable hydrogen atom donors (reactions (1)–(4)). The photodegradation rate of the unidentified chromophore in the brown LSOM is similarly affected by viscosity. However, we want to emphasize that not all organic photochemical reactions will be suppressed in viscous aerosols by the same mechanism. Direct photolysis processes occur on faster time scales and do not require the excited molecules to diffuse through the matrix before the reaction. Such reactions are less likely to be affected by the material viscosity; for example, Norrish-I splitting of carbonyls can be efficient even in crystals.⁷⁵ On the other hand, caging effects could be more significant in highly-viscous solvents, and result in suppression of direct photolysis quantum yields. Therefore, the effects of viscosity on photochemical reactions need to be investigated on a case by case basis.

These results could help in the interpretation of atmospheric lifetimes of particulate nitro-aromatic compounds, some of which are known toxins. In cold and dry segments of the atmosphere, such as over the polar regions and near the tropopause, these compounds could survive longer if they are trapped inside highly-viscous particles. In contrast, the same compounds could degrade faster under warm, humid conditions or when they are unprotected on the particle surface. It is possible that other types of photolabile organic compounds can similarly be protected from photodegradation under cold, dry conditions. It is also possible that photosensitized reactions can similarly be suppressed by the viscosity of the SOM matrix. These effects will need to be investigated in future studies. It also remains to be seen if these conclusions can be applied to other types of SOA, including those formed from anthropogenic sources.

Conclusions

In our previous work,²⁵ we found that the photodegradation rate of 2,4-DNP in viscous PSOM had a significantly stronger temperature dependence than the same process in much less viscous octanol. We suggested that this effect was due to the

fact that temperature has a stronger effect on the viscosity of PSOM than on the viscosity of octanol. The increased viscosity may be hindering the motion of electronically excited 2,4-DNP molecules within SOM, slowing its photodegradation. In order to examine this effect, we expanded the scope of the previous measurements to investigate the effect of relative humidity on the photodegradation kinetics of 2,4-DNP in PSOM. We also investigated LSOM as an alternative organic matrix for 2,4-DNP photodegradation, and carried out similar experiments with a completely different photochemical system, specifically brown LSOM obtained by exposure of LSOM to ammonia. In all cases, as the viscosity of the SOM was increased by cooling the material or exposing it to dry air, the reaction rate decreased. The activation energy for the 2,4-DNP photodegradation in PSOM and LSOM were correlated with the explicitly measured viscosity of the materials.

Acknowledgements

P. L., A. L., J. L., and S. N. acknowledge support by the U.S. Department of Commerce, National Oceanic and Atmospheric Administration through Climate Program Office's AC4 program, awards NA13OAR4310066 (PNNL) and NA13OAR4310062 (UCI). MH and HL acknowledge support by the National Science Foundation (NSF) grant CHE-0909227. MB was supported by the NSF summer research undergraduate experience (RUE) program. MS, JG, and AB were supported by the Natural Sciences and Engineering Research Council of Canada. The LC-PDA-MS measurements were performed at the W. R. Wiley Environmental Molecular Sciences Laboratory (EMSL), a national scientific user facility located at PNNL, and sponsored by the Office of Biological and Environmental Research of the US. DOE. PNNL is operated for US DOE by Battelle Memorial Institute under Contract No. DEAC06-76RL0 1830.

References

- 1 C. Kidd, V. Perraud, L. M. Wingen and B. J. Finlayson-Pitts, *Proc. Natl. Acad. Sci. U. S. A.*, 2014, **111**, 7552–7557.
- 2 T. Koop, J. Bookhold, M. Shiraiwa and U. Poeschl, *Phys. Chem. Chem. Phys.*, 2011, **13**, 19238–19255.
- 3 L. Renbaum-Wolff, J. W. Grayson, A. P. Bateman, M. Kuwata, M. Sellier, B. J. Murray, J. E. Shilling, S. T. Martin and A. K. Bertram, *Proc. Natl. Acad. Sci. U. S. A.*, 2013, **110**, 8014–8019.
- 4 A. Virtanen, J. Joutsensaari, T. Koop, J. Kannosto, P. Yli-Pirila, J. Leskinen, J. M. Makela, J. K. Holopainen, U. Poeschl, M. Kulmala, D. R. Worsnop and A. Laaksonen, *Nature*, 2010, **467**, 824–827.
- 5 A. P. Bateman, A. K. Bertram and S. T. Martin, *J. Phys. Chem. A*, 2015, **119**, 4386–4395.
- 6 V. Perraud, E. A. Bruns, M. J. Ezell, S. N. Johnson, Y. Yu, M. L. Alexander, A. Zelenyuk, D. Imre, W. L. Chang, D. Dabdub, J. F. Pankow and B. J. Finlayson-Pitts, *Proc. Natl. Acad. Sci. U. S. A.*, 2012, **109**, 2836–2841.
- 7 R. A. Zaveri, R. C. Easter, J. E. Shilling and J. H. Seinfeld, *Atmos. Chem. Phys. Discuss.*, 2013, **13**, 28631–28694.
- 8 T. D. Vaden, D. Imre, J. Beránek, M. Shrivastava and A. Zelenyuk, *Proc. Natl. Acad. Sci. U. S. A.*, 2011, **108**, 2190–2195.
- 9 M. Shiraiwa, A. Zuend, A. K. Bertram and J. H. Seinfeld, *Phys. Chem. Chem. Phys.*, 2013, **15**, 11441–11453.
- 10 I. Riipinen, J. R. Pierce, T. Yli-Juuti, T. Nieminen, S. Häkkinen, M. Ehn, H. Junninen, K. Lehtipalo, T. Petäjä, J. Slowik, R. Chang, N. C. Shantz, J. Abbatt, W. R. Leitch, V. M. Kerminen, D. R. Worsnop, S. N. Pandis, N. M. Donahue and M. Kulmala, *Atmos. Chem. Phys.*, 2011, **11**, 3865–3878.
- 11 D. L. Bones, J. P. Reid, D. M. Lienhard and U. K. Krieger, *Proc. Natl. Acad. Sci. U. S. A.*, 2012, **109**, 11613–11618.
- 12 M. Shiraiwa, M. Ammann, T. Koop and U. Pöschl, *Proc. Natl. Acad. Sci. U. S. A.*, 2011, **108**, 11003–11008.
- 13 B. Wang, R. E. O'Brien, S. T. Kelly, J. E. Shilling, R. C. Moffet, M. K. Gilles and A. Laskin, *J. Phys. Chem. A*, 2015, **119**, 4498–4508.
- 14 H. C. Price, J. Mattsson, Y. Zhang, A. K. Bertram, J. F. Davies, J. W. Grayson, S. T. Martin, D. O'Sullivan, J. P. Reid, A. M. J. Rickards and B. J. Murray, *Chem. Sci.*, 2015, **6**, 4876–4883.
- 15 A. Zelenyuk, D. Imre, J. Beránek, E. Abramson, J. Wilson and M. Shrivastava, *Environ. Sci. Technol.*, 2012, **46**, 12459–12466.
- 16 R. M. Power, S. H. Simpson, J. P. Reid and A. J. Hudson, *Chem. Sci.*, 2013, **4**, 2597–2604.
- 17 J. D. Hearn and G. D. Smith, *Phys. Chem. Chem. Phys.*, 2005, **7**, 2549–2551.
- 18 D. A. Knopf, L. M. Anthony and A. K. Bertram, *J. Phys. Chem. A*, 2005, **109**, 5579–5589.
- 19 M. Kuwata and S. T. Martin, *Proc. Natl. Acad. Sci. U. S. A.*, 2012, **109**, 17354–17359.
- 20 S. Zhou, M. Shiraiwa, R. D. McWhinney, U. Pöschl and J. P. D. Abbatt, *Faraday Discuss.*, 2013, **165**, 391–406.
- 21 V. Perraud, E. A. Bruns, M. J. Ezell, S. N. Johnson, Y. Yu, M. L. Alexander, A. Zelenyuk, D. Imre, W. L. Chang, D. Dabdub, J. F. Pankow and B. J. Finlayson-Pitts, *Proc. Natl. Acad. Sci. U. S. A.*, 2012, **109**, 2836–2841.
- 22 H. C. Price, B. J. Murray, J. Mattsson, D. O'Sullivan, T. W. Wilson, K. J. Baustian and L. G. Benning, *Atmos. Chem. Phys.*, 2014, **14**, 3817–3830.
- 23 M. Song, P. Liu, S. Hanna, S. Martin and A. Bertram, *Atmos. Chem. Phys. Discuss.*, 2015, **15**, 1131–1169.
- 24 A. P. Bateman, H. Belassein and S. T. Martin, *Aerosol Sci. Technol.*, 2013, **48**, 42–52.
- 25 H. Lignell, M. L. Hinks and S. A. Nizkorodov, *Proc. Natl. Acad. Sci. U. S. A.*, 2014, **111**, 13780–13785.
- 26 R. K. Pathak, A. A. Presto, T. E. Lane, C. O. Stanier, N. M. Donahue and S. N. Pandis, *Atmos. Chem. Phys.*, 2007, **7**, 3811–3821.
- 27 T. Wainman, J. Zhang, C. J. Weschler and P. J. Liroy, *Environ. Health Perspect.*, 2000, **108**, 1139–1145.
- 28 H. J. Lee, P. K. Aiona, A. Laskin, J. Laskin and S. A. Nizkorodov, *Environ. Sci. Technol.*, 2014, **48**, 10217–10226.

- 29 D. E. Romonosky, A. Laskin, J. Laskin and S. A. Nizkorodov, *J. Phys. Chem. A*, 2015, **119**, 2594–2606.
- 30 A. Laskin, J. Laskin and S. A. Nizkorodov, *Chem. Rev.*, 2015, **115**, 4335–4382.
- 31 C. George, M. Ammann, B. D'Anna, D. J. Donaldson and S. A. Nizkorodov, *Chem. Rev.*, 2015, **115**, 4218–4258.
- 32 P. J. Shea, J. B. Weber and M. R. Overcash, in *Residue Reviews*, ed. F. Gunther and J. Gunther, Springer, New York, 1983, vol. 87, ch. 1, pp. 1–41.
- 33 M. M. Sanagi, M. Miskam, W. A. Wan Ibrahim, D. Hermawan and H. Y. Aboul-Enein, *J. Sep. Sci.*, 2010, **33**, 2131–2139.
- 34 A. Albinet, C. Minero and D. Vione, *Chemosphere*, 2010, **80**, 753–758.
- 35 M. A. J. Harrison, S. Barra, D. Borghesi, D. Vione, C. Arsene and R. Iulian Olariu, *Atmos. Environ.*, 2005, **39**, 231–248.
- 36 M. Takezaki, N. Hirota and M. Terazima, *J. Phys. Chem. A*, 1997, **101**, 3443–3448.
- 37 K. M. Updyke, T. B. Nguyen and S. A. Nizkorodov, *Atmos. Environ.*, 2012, **63**, 22–31.
- 38 T. B. Nguyen, P. B. Lee, K. M. Updyke, D. L. Bones, J. Laskin, A. Laskin and S. A. Nizkorodov, *J. Geophys. Res.: Atmos.*, 2012, **117**, D01207.
- 39 D. L. Bones, D. K. Henricksen, S. A. Mang, M. Gonsior, A. P. Bateman, T. B. Nguyen, W. J. Cooper and S. A. Nizkorodov, *J. Geophys. Res.: Atmos.*, 2010, **115**, D05203.
- 40 T. B. Nguyen, A. Laskin, J. Laskin and S. A. Nizkorodov, *Faraday Discuss.*, 2013, **165**, 473–494.
- 41 S. L. Clegg, P. Brimblecombe and A. S. Wexler, *J. Phys. Chem. A*, 1998, **102**, 2137–2154.
- 42 J. W. Grayson, M. Song, M. Sellier and A. K. Bertram, *Atmos. Meas. Tech. Discuss.*, 2015, **8**, 877–903.
- 43 B. J. Murray, A. E. Haddrell, S. Peppe, J. F. Davies, J. P. Reid, D. O'Sullivan, H. C. Price, R. Kumar, R. W. Saunders, J. M. C. Plane, N. S. Umo and T. W. Wilson, *Atmos. Chem. Phys.*, 2012, **12**, 8575–8587.
- 44 M. Song, C. Marcolli, U. K. Krieger, A. Zuend and T. Peter, *Atmos. Chem. Phys.*, 2012, **12**, 2691–2712.
- 45 T. Koop, A. Kapilashrami, L. T. Molina and M. J. Molina, *J. Geophys. Res.: Atmos.*, 2000, **105**, 26393–26402.
- 46 A. K. Bertram, S. T. Martin, S. J. Hanna, M. L. Smith, A. Bodsworth, Q. Chen, M. Kuwata, A. Liu, Y. You and S. R. Zorn, *Atmos. Chem. Phys.*, 2011, **11**, 10995–11006.
- 47 P. C. Reist, *Aerosol science and technology*, McGraw-Hill, 1993.
- 48 E. Schnell, *J. Appl. Phys.*, 1956, **27**, 1149–1152.
- 49 N. V. Churaev, V. D. Sobolev and A. N. Somov, *J. Colloid Interface Sci.*, 1984, **97**, 574–581.
- 50 K. Watanabe and H. Udagawa, *AIChE J.*, 2001, **47**, 256–262.
- 51 J. Baudry, E. Charlaix, A. Tonck and D. Mazuyer, *Langmuir*, 2001, **17**, 5232–5236.
- 52 V. S. J. Craig, C. Neto and D. R. M. Williams, *Phys. Rev. Lett.*, 2001, **87**, 054504.
- 53 D. C. Trethewey and C. D. Meinhart, *Phys. Fluids*, 2002, **14**, L9–L12.
- 54 J. T. Cheng and N. Giordano, *Phys. Rev. E: Stat., Nonlinear, Soft Matter Phys.*, 2002, **65**, 031206.
- 55 S. Jin, P. Huang, J. Park, J. Y. Yoo and K. S. Breuer, *Exp. Fluids*, 2004, **37**, 825–833.
- 56 P. Joseph and P. Tabeling, *Phys. Rev. E: Stat., Nonlinear, Soft Matter Phys.*, 2005, **71**, 035303.
- 57 N. Chiara, R. E. Drew, B. Elmar, B. Hans-Jürgen and S. J. C. Vincent, *Rep. Prog. Phys.*, 2005, **68**, 2859.
- 58 C.-H. Choi and C.-J. Kim, *Phys. Rev. Lett.*, 2006, **96**, 066001.
- 59 L. Joly, C. Ybert and L. Bocquet, *Phys. Rev. Lett.*, 2006, **96**, 046101.
- 60 L. Zhu, C. Neto and P. Attard, *Langmuir*, 2012, **28**, 3465–3473.
- 61 L. Li, J. Mo and Z. Li, *Phys. Rev. E: Stat., Nonlinear, Soft Matter Phys.*, 2014, **90**, 033003.
- 62 R. Tuckermann and H. K. Cammenga, *Atmos. Environ.*, 2004, **38**, 6135–6138.
- 63 G. J. Engelhart, A. Asa-Awuku, A. Nenes and S. N. Pandis, *Atmos. Chem. Phys.*, 2008, **8**, 3937–3949.
- 64 X. Chen and P. K. Hopke, *Indoor Air*, 2009, **19**, 335–345.
- 65 E. Kostenidou, R. K. Pathak and S. N. Pandis, *Aerosol Sci. Technol.*, 2007, **41**, 1002–1010.
- 66 R. Zhao, A. K. Y. Lee, L. Huang, X. Li, F. Yang and J. P. D. Abbatt, *Atmos. Chem. Phys. Discuss.*, 2015, **15**, 2957–2996.
- 67 H. Forrister, J. Liu, E. Scheuer, J. Dibb, L. Ziemba, K. L. Thornhill, B. Anderson, G. Diskin, A. E. Perring, J. P. Schwarz, P. Campuzano-Jost, D. A. Day, B. B. Palm, J. L. Jimenez, A. Nenes and R. J. Weber, *Geophys. Res. Lett.*, 2015, **42**, 2015GL063897.
- 68 A. Laskin, J. Laskin and S. A. Nizkorodov, *Chem. Rev.*, 2015, **115**, 4335–4382.
- 69 J. F. Pankow, *Atmos. Environ.*, 2003, **37**, 3323–3333.
- 70 M. D. Petters, S. M. Kreidenweis, J. R. Snider, K. A. Koehler, Q. Wang, A. J. Prenni and P. J. Demott, *Tellus, Ser. B*, 2006, **58**, 196–205.
- 71 S. Liu, J. E. Shilling, C. Song, N. Hiranuma, R. A. Zaveri and L. M. Russell, *Aerosol Sci. Technol.*, 2012, **46**, 1359–1369.
- 72 H. J. Tong, J. P. Reid, D. L. Bones, B. P. Luo and U. K. Krieger, *Atmos. Chem. Phys.*, 2011, **11**, 4739–4754.
- 73 D. J. Burnett, F. Thielmann and J. Booth, *Int. J. Pharm.*, 2004, **287**, 123–133.
- 74 B. Zobrist, V. Soonsin, B. P. Luo, U. K. Krieger, C. Marcolli, T. Peter and T. Koop, *Phys. Chem. Chem. Phys.*, 2011, **13**, 3514–3526.
- 75 M. A. Garcia-Garibay and L. M. Campos, *ChemInform*, 2004, **35**, DOI: 10.1002/chin.200419246.